Journal of Medicinal Chemistry

Article

pubs.acs.org/jmc

Identification of Potent and Selective Hydantoin Inhibitors of Aggrecanase-1 and Aggrecanase-2 That Are Efficacious in Both Chemical and Surgical Models of Osteoarthritis

Timothy B. Durham,* Valentine J. Klimkowski, Christopher J. Rito, Jothirajah Marimuthu, James L. Toth, Chin Liu, Jim D. Durbin, Stephanie L. Stout, Lisa Adams, Craig Swearingen, Chaohua Lin, Mark G. Chambers, Kannan Thirunavukkarasu, and Michael R. Wiley

Eli Lilly and Company, Lilly Corporate Center, Indianapolis, Indiana 46285, United States

Supporting Information

ABSTRACT: A disintegrin and metalloproteinase with thrombospondin motifs-4 (ADAMTS-4) and ADAMTS-5 are zinc metalloproteases commonly referred to as aggrecanase-1 and aggrecanase-2, respectively. These enzymes are involved in the degradation of aggrecan, a key component of cartilage. Inhibitors of these enzymes could be potential osteoarthritis (OA) therapies. A series of hydantoin inhibitors of ADAMTS-4 and ADAMTS-5 were identified from a screening campaign and optimized through structure-based drug design to give hydantoin **13**. Hydantoin **13** had excellent selectivity over other zinc metalloproteases such as TACE, MMP2, MMP3, MMP13, and MMP14. The compound also produced efficacy in both a chemically induced and surgical model of OA in rats.

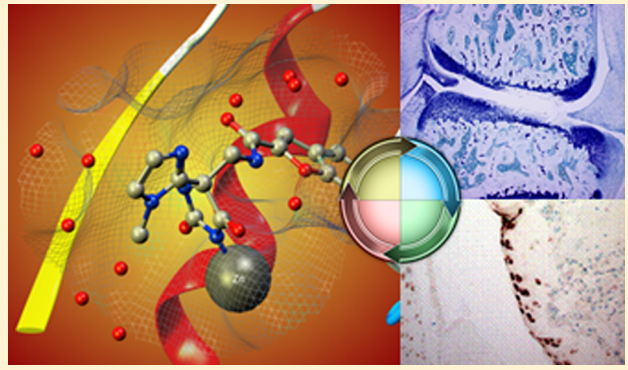

INTRODUCTION

Osteoarthritis (OA) is a disease characterized by the degradation of the joint cartilage leading to pain and loss of joint function. The disease is widespread, with estimates suggesting that in 2008 there were at least 27 million people in the U.S. with some form of OA.[1] Worldwide estimates place the percentage of the population over the age of 60 with symptomatic OA as 9.6% for men and 18% for women.[2] Studies have found that radiographic OA of the knee in persons 45 years of age and older in the U.S. and Europe is widespread and affects 14% of men and 23% of women.[3] The societal impact of this disease is significant, leading to a major economic burden on the world's healthcare systems and significant compromises in quality of life.[4] Currently, the main course of treatment for OA patients involves symptom relief through the use of NSAIDS and, when that becomes no longer effective, joint replacement surgery. Unfortunately, there is no approved treatment regimen that can directly affect the progression of OA. Therefore, a disease-modifying OA drug (DMOAD) would be a valuable asset to patients and care givers.

The joint contains both cartilage and synovial fluid. Synovial fluid is a non-Newtonian fluid composed primarily of water, hyaluronic acid, and the glycosylated peptide lubricin. Synovial fluid is responsible for the transport of nutrients to and waste products out of the joint space. This exchange process between synovial fluid and plasma is believed to be diffusion-controlled.[5]

Cartilage is nonvascularized tissue composed of two major components: type II collagen and aggrecan. Type II collagen is an extracellular matrix (ECM) protein that forms cross-linked rigid triple helices. These helices provide strength to the cartilage. Aggrecan is an extensively glycosylated ECM protein that provides compressibility. Aggrecan has two globular structural domains (designated G1 and G2) at the N-terminus and a third globular domain (G3) at the C-terminus.[6] Between the G2 and G3 domains, the protein is highly glycosylated, with >100 glycosyl chains attached. The glycolsylated core of the protein is highly hydrated. It is this high level of hydration that provides the compressibility to cartilage.

The ECM proteins in cartilage are synthesized by chondrocytes located within the cartilage matrix. In the normal process of tissue remodeling, the ECM proteins are later degraded by a number of proteases. One hypothesis for how OA progresses is that the rate of ECM synthesis versus degradation becomes unbalanced when an insult to the system occurs. Thus, inhibitors of ECM proteases could provide an effective means to halt or even reverse the progression of OA. In this context, several proteases could be potential drug targets due to their propensity to degrade collagen.[7] Multiple members of the matrix metalloprotease (MMP) family meet this criteria.[8] MMPs are zinc metalloproteases. There are 28 MMPs known, all of which have a high level of homology around the catalytic site. The MMPs have been implicated not only in degradation of collagen but also in the degradation of a variety other

Received: October 5, 2014

   dx.doi.org/10.1021/jm501522n | J. Med. Chem. XXXX, XXX, XXX−XXX

biomolecules important to disease and normal physiological processes.[9] However, broad spectrum MMP inhibitors have been unsuccessful in clinical applications for a variety of indications due to musculoskeletal syndrome (MSS), a reversible fibromyalgia that causes pain and swelling in the joints.[10]

ADAMTS-4 (a disintegrin and metalloproteinase with thrombospondin motifs-4) and ADAMTS-5 are commonly referred to as aggrecanase-1 and aggrecanase-2, respectively. ADAMTS-4 and ADAMTS-5 are zinc metalloproteases that, unlike the MMPs, are known to have a specific and primary role in aggrecan degradation. Both aggrecanases cleave the Glut373−Ala374 peptide bond located between the G1 and G2 domains.[11] This cleavage is the first step in aggrecan degradation. Since aggrecan is responsible for cartilage's compressibility, aggrecan loss would be expected to increase the mechanical trauma that the joint undergoes during movement, leading to structural damage and inflammation. In support of this hypothesis, ADAMTS-5$^{-/-}$ mice show protection against both chemical and surgical models of OA.[12] Furthermore, mice genetically modified to express a form of aggrecan that is resistant to cleavage by ADAMTS-5 are also protected against models of OA compared to WT mice.[13] Interestingly, ADAMTS-4$^{-/-}$ mice do not show protection against OA models, suggesting that, in mice, ADAMTS-5 is the more relevant protease for aggrecan cleavage.[14] However, in human chrondrocytes, siRNA transfection to decrease expression of either ADAMTS-4 or ADAMTS-5 resulted in reduced aggrecan cleavage, suggesting that, in humans, both enzymes may be important in aggrecan degradation.[15]

The above data point to ADAMTS-4 and ADAMTS-5 as being interesting potential targets for DMOAD research. However, the active sites of ADAMTS-4 and ADAMTS-5 share significant similarity with the MMPs in that all of the enzymes contain a HExxHxxGxxH zinc-binding motif. Most of the previously reported inhibitors of ADAMTS-4 and ADAMTS-5 do not show significant selectivity over the other MMPs or come from the chemical classes of hydroxamic acids or sulfonamides that can be challenging platforms for the development of oral drugs.[16] Therefore, our goal was to identify nonhydroxamate/sulfonamide inhibitors of ADAMTS-4 and ADAMTS-5 with suitable potency and pharmacokinetics to determine if chronic and selective inhibition of these enzymes would result in modification of the degenerative process in OA disease models similar to the phenotypes observed in knockout animals.

RESULTS AND DISCUSSION

To initiate our research effort, we carried out a biochemical screen of 80 000 structurally diverse compounds to identify potential starting points for inhibitor development. From that screening campaign, we identified hydantoin **1** as an interesting dual inhibitor (Figure 1). Hydantoin **1** showed modest inhibition of hADAMTS-4 and hADAMTS-5 enzymes (IC_{50} of 74 and 350 nM, respectively) as well as modest selectivity over several zinc metalloproteases (Table 1). Furthermore, hydantoin **1** and all of its subsequent analogues described herein had essentially equipotent activity (<2-fold shift) against rADAMTS-5.

Because the joint space contains large biopolymers (vide supra), we wanted to understand if nonspecific protein binding could limit the functional activity of our inhibitors. However, developing a routine assay in synovial fluid was technically challenging. Therefore, we decided to use a modified enzyme assay run in the presence of 50% rat plasma as a tool for assessing the effects of nonspecific protein binding; compound **1** had modest activity in the presence of rat plasma. It also had low oral exposure in rats, necessitating the need to further optimize pharmacokinetic performance in rodents.

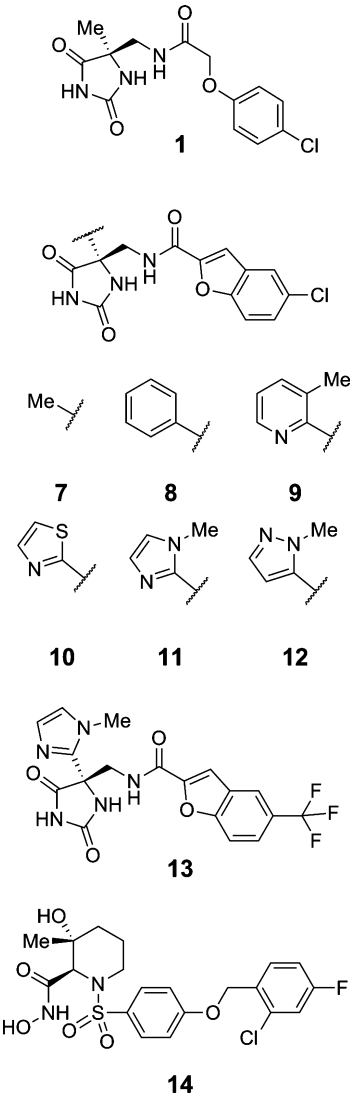

Figure 1. Inhibitors of ADMTS-4 and ADAMTS-5.

We were able to co-crystallize compound **1** with hADAMTS-4 (Figure 2), which allowed us to clearly understand the mode of ligand binding. The hydantoin ring forms critical polar interactions with the protein at three of its five positions. The imide nitrogen of the hydantoin ring interacts directly with the catalytic zinc. In addition, the hydantoin ring forms four hydrogen-bonding interactions with structural water, the carbonyl of Gly331, and the carboxyl of Glu362. The amide linker also forms hydrogen bonds with Leu330 and Pro393. The 4-chlorophenoxy ring is directed into the hydrophobic S1′ pocket, whereas the C5 methyl group of the hydantoin is directed toward the S1 region.

Upon examination of the X-ray co-crystal structure of hydantoin **1**, we anticipated that an improvement in compound potency could be achieved through fusion of the phenoxy acetyl group into a benzofuran, thereby limiting the degrees of conformational freedom in the ligand. We anticipated that this

dx.doi.org/10.1021/jm501522n | J. Med. Chem. XXXX, XXX, XXX−XXX

Table 1. Biochemical Activity and Rat Oral Exposure of ADAMTS-4 and ADAMTS-5 Inhibitors[a]

compd	hADAMTS-4 IC_{50} (nM)	hADAMTS-5 IC_{50} (nM)	rat plasma[b] hADAMTS-5 IC_{50} (nM)	hMMP2 IC_{50} (nM)	hMMP3 IC_{50} (nM)	hMMP13 IC_{50} (nM)	hMMP14 IC_{50} (nM)	hTACE IC_{50} (nM)	2 h plasma (ng/mL)[c]	8 h Plasma (ng/mL)[c]
1	74	350	620	24 000	50 000	7000	>50 000	ND	430	50
7[d]	110	150	2400	ND	ND	ND	ND	ND	ND	ND
8	12	22	420	2100	3000	720	3500	5400	<200	ND
9[d]	17	19	1700	6100	20 000	3100	18 000	ND	ND	ND
10	8	17	330	1800	1900	930	870	10 000	4300	1300
11	5	9	110	7500	38 000	4200	>100 000	ND	2200	80
12[d]	22	19	530	7100	64 000	4700	8600	ND	ND	ND
13	4	4	35	11 000	69 000	30 000	86 000	10 000	1100	90
14	1	1	18	5	3	1	150	7	1900	840

[a]All values are relative IC_{50}'s. The IC_{50} data for ADAMTS-4 and ADAMTS-5 are mean values generated from at least $n = 3$. [b]Rat plasma IC_{50}'s were generated using hADAMTS-5 under standard assay conditions run in the presence of 50% rat plasma. [c]Plasma levels are mean values generated in $n = 3$ rats after a 10 mg/kg PO dose. Compounds were extracted from plasma using acetonitrile and quantified by MS. [d]Data shown is for the racemate. ND, not determined.

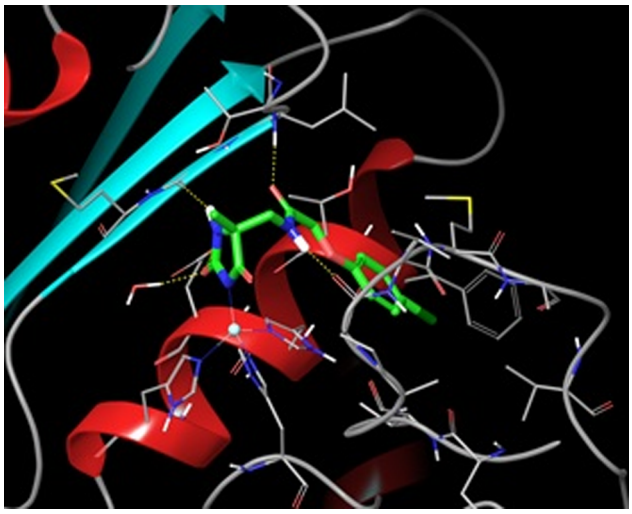

Figure 2. X-ray co-crystal structure of hydantoin **1** with hADAMTS-4. Zinc is shown as a blue sphere. Resolution = 1.24 Å.

should also improve the stereoelectronic interactions between the His361 imidazole ligating the catalytic zinc and the ligand π-system. Benzofuran **7** showed improved potency against ADAMTS-5 with no loss in ADAMTS-4 potency (Figure 1 and Table 1).

We next sought further potency improvement and hoped that we could enhance the pharmacokinetic performance of the molecules through optimization of the P1 substituent. We also saw the P1 substituent as a promising position to modulate physical properties such as solubility and polarity to fine-tune the molecules' performance characteristics. Synthesis of analogues of compound **1** was straightforward and began with introduction of the P1 substituent through addition of either a Grignard reagent or organolithium species to the Weinreb amide of Boc-glycine to produce aminoketone **3** (Scheme 1). We next carried out a Bucherer–Burge reaction to give hydantoin **4**.[17] The hydantoins were easily resolved via chiral chromatography to the more active stereo isomer **5**. Deprotection to give amine **6** and subsequent amide formation produced hydantoins **7**–**13** (Figure 1).

As the size of the P1 substituent was increased from methyl (**7**) to phenyl (**8**), we saw a 10× improvement in biochemical potency against ADAMTS-4 and ADAMTS-5 (Table 1). However, compound **8** had low oral exposure in rats and suffered from limited selectivity against other metalloproteases.

Scheme 1. Synthesis of Hydantoins 7–13[a]

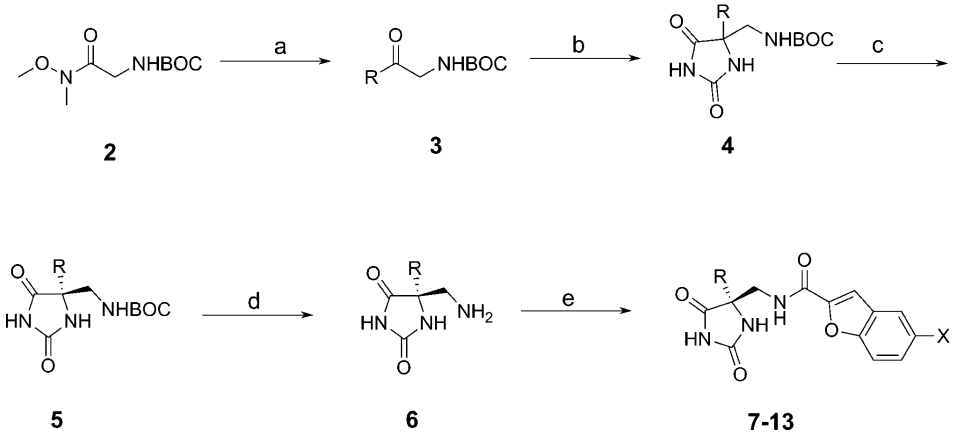

[a]Conditions: (a) M-R (2 equiv; M = MgBr, MgCl, or Li), THF, −78 °C to ambient temperature, 20–96%; (b) KCN, $(NH_4)_2CO_3$, MeOH/water 1:1, heat, 23–85%; (c) chiral chromatography; (d) HCl·dioxane, MeOH, quant.; (e) PyBrop, DIPEA, appropriate benzofuran carboxylix acid, DMF, 25–66% over three steps.

dx.doi.org/10.1021/jm501522n | J. Med. Chem. XXXX, XXX, XXX–XXX

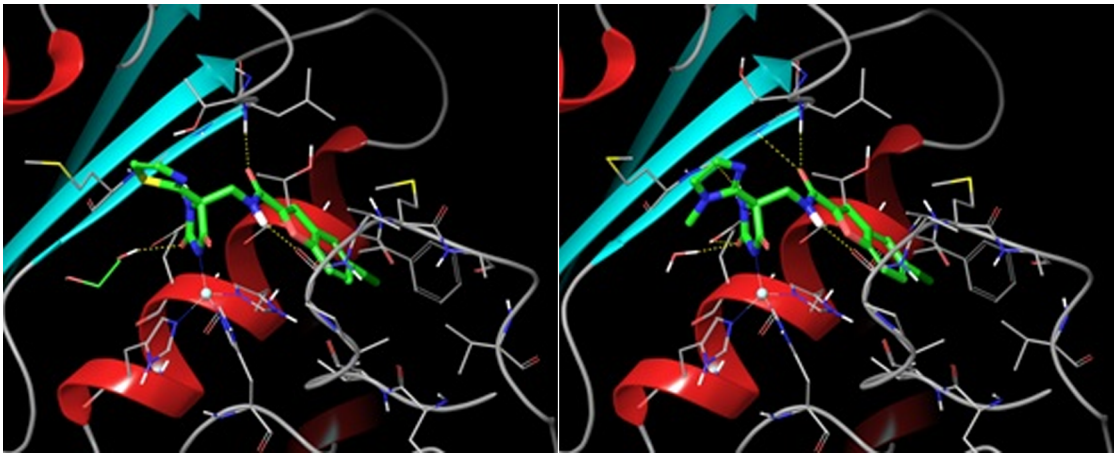

Figure 3. X-ray co-crystal structures of compounds **10** (left) and **11** (right) with hADAMTS-4. Zinc is shown as a blue sphere. Resolution =1.62 and 1.60 Å, respectively.

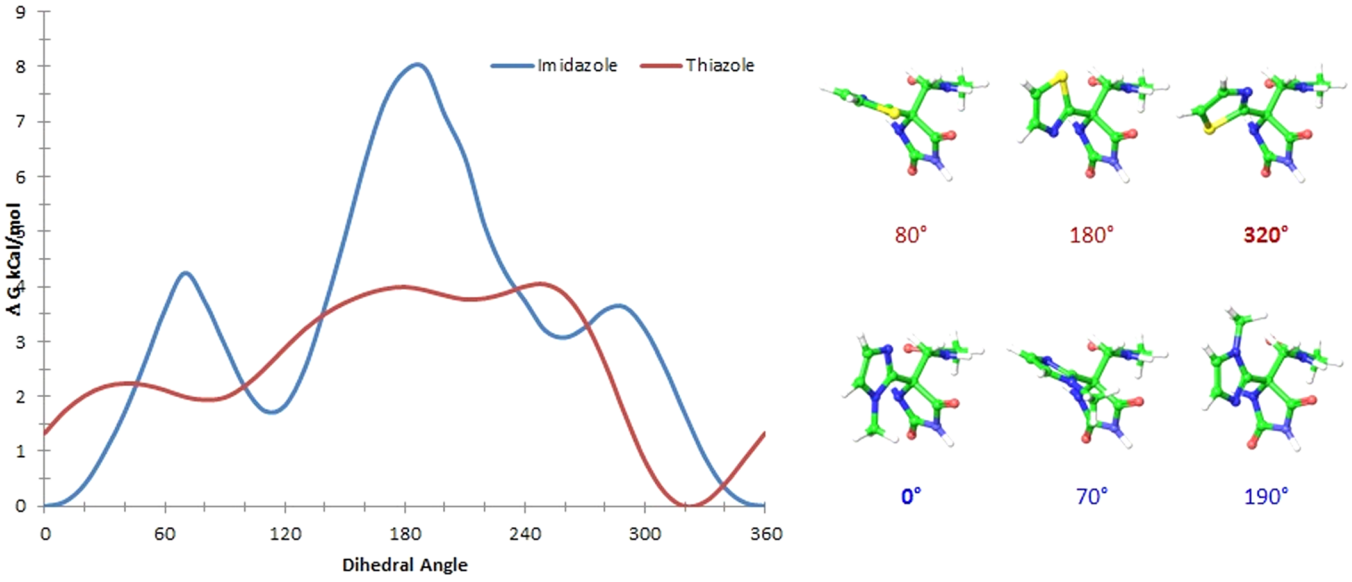

Figure 4. Calculated Δ*G* vs dihedral angle for model hydantoin system. The graph shows Δ*G* versus dihedral angle for a model system of hydantoins **10** and **11**. In the model, the benzofuran was replaced with a simple acetyl side chain. Key conformations are shown on the right, with the corresponding dihedral angle given below. Global minima are indicated in bold.

Therefore, we set out to further improve our hydantoin inhibitors by increasing their plasma activity, metalloprotease selectivity, and oral exposure in rats. We hypothesized that replacing the phenyl ring of hydantoin **8** with a heterocycle could improve functional activity by lowering protein binding as well as limiting oxidative metabolism, thus improving exposure. To that end, we prepared the series of heterocyclic replacements for the phenyl ring shown in Table 1 (compounds **9**–**12**).

Replacement of phenyl with a pyridyl substituent to give hydantoin **9** resulted in gains in metalloprotease selectivity. Furthermore, replacement of the pyridine with five-membered heterocycles greatly impacted the pharmacokinetic performance of the hydantoins. Thiazole **10** had potent activity against both hADAMTS-4 and hADAMTS-5, with a rat plasma IC_{50} of 330 nM. It also displayed exceptional oral exposure (Tables 1 and 2). Thiazole **10** has only modest selectivity over the other metaloproteases shown in Table 1. Therefore, we sought to improve our selectivity profile while maintaining good oral exposure properties.

To that end, we next explored imidazole and pyrazole as heterocyclic P1 groups. Compound **11** provided our most encouraging results. Compound **11** not only improved plasma potency relative to that of thiazole **10** but also showed enhanced selectivity against the other zinc metalloproteases. Furthermore, we were delighted to see that imidazole **11** still maintained reasonable oral exposure.

The subtlety of the SAR within this limited set of compounds for both plasma activity and metalloprotease selectivity is intriguing. In comparing compound **10** to **11**, we see that the simple change from thiazole to imidazole leads to an increase in metalloprotease selectivity. This is due to two factors. One is a very small improvement in potency against ADAMTS-5 going from compound **10** to **11**. The second factor is a loss in potency against our panel metalloproteases, which in the case of MMP3 and MMP14 was greater than 10-fold. To better understand the difference in compound performance, we obtained X-ray co-crystal structures for compounds **10** and **11** in hADAMTS-4 (Figure 3). The X-ray data reveal that the only significant change in binding between the two compounds

dx.doi.org/10.1021/jm501522n | *J. Med. Chem.* XXXX, XXX, XXX–XXX

is the orientation of the heterocyclic substituent such that the imidazole is rotated approximately 45° out of the plane occupied by the thiazole ring.

To investigate why such a significant difference in orientation was observed, we performed quantum mechanical calculations to explore the energetic barrier to rotation for the respective heterocycles. Gas-phase calculations at the B3YP/6-31G* level allowed us to estimate the energy rotation barriers for two model hydantoin compounds (Figure 4). Notably, we observed that both thiazole **10** and imidazole **11** bind to ADAMTS-4 with their heterocyles in their respective global minima. Furthermore, we noted that imidazole **11** has a larger barrier to rotation than that of thiazole **10**. This can be explained primarily by increased steric interactions of the imidazole ring methyl substituent with both the hydantoin ring and the amide linker.

Published crystal structures of hMMP14 (1BQQ)[18] and hMMP3 (1G4K)[19] show subtle differences in amino acid composition and protein structure in the S1 pocket relative to that of ADAMTS4. We believe that for hydantoin **11** it is the combination of the energetic barrier to rotation, the unique electronic character of the imidazole ring, and the structural differences between the enzymes that leads to the enhanced selectivity relative to that of thiazole **10**. The hypothesis that selectivity is being controlled by a subtle balance of multiple characteristics of the P1 heterocyclic substituent is supported by the observation that pyrrazole **12**, which differs from imiadazole **11** only in the position of a nitrogen atom, has slightly higher MMP3 selectivity but significantly lower MMP14 selectivity relative to that of imidazole **11**.

While compound **11** demonstrated significantly improved rat oral exposure and selectivity relative to that of compound **1**, we still hoped that we could improve potency and selectivity within the series further by subtle manipulation of the benzofuran. Replacement of the chloro substituent of compound **11** with a trifluoromethyl group produced compound **13**, which had increased plasma potency as well as improved selectivity against MMP13 and MMP14 (Table 1). Compound **13** also maintained the positive rat pharmacokinetics of compound **11**, thus showing an overall improved set of performance characteristics (Table 2). Compound **13** also had good microsomal stability properties and did not show significant inhibition of key human microsomes (Table 3). Compound **13**, therefore, met our needs as a selective tool for proof-of-concept work in vivo.

Table 2. Rat Pharmacokinetics of Hydantoins 10, 11, and 13[a]

compd	10	11	13
AUC (ng h/mL)[b]	28 000	8100	8500
C_{max} (ng/mL)[b]	6900	4100	3200
T_{max} (h)[b]	0.33	0.33	1.6
$T_{1/2}$ (h)[b]	3.2	4.2	4.3
Cl (mL/min/kg)	4.0	13	4.8
%F	72	58	25

[a]All data generated in SD rats. Values are an average of $n = 3$ animals. [b]Data reported using a 10 mg/kg PO dose.

Compounds **10**, **11**, and **13** provided us with an ideal opportunity to explore the outcome of ADAMTS-4 and ADAMTS-5 inhibition in rats with both highly selective (compound **13**) and less selective (compound **10**) inhibitors.

Table 3. Microsomal Data for Compounds 10, 11, and 13

compd	hCyp2D6 inhibition (%)	hCyp2C9 inhibition (%)	hCyp3A4 inhibition (%)	human microsomal metabolism (%)[a]	rat microsomal metabolism (%)[a]
10	12	6	<5	16	16
11	<5	<5	<5	17	13
13	<5	<5	<5	<5	7

[a]Values show the percentage of compound degraded by microsomes over 30 min at 37 °C, as determined by LC-MS.

We previously reported a pharmacodynamic model of aggrecanase activity in which injection of monoiodoacetate (MIA) directly into the joint of the animal induces the release of proteases, including ADAMTS-4 and ADAMTS-5, which lead to degradation of the cartilage over a 5 day period.[20] We also disclosed novel ELISA assays that can be used in conjunction with the above model to measure the direct products of ADAMTS-4 and ADAMTS-5 cleavage of aggrecan in synovial fluid.[21]

Compounds **10**, **11**, and **13** produced statistically significant reductions in ADAMTS-4/ADAMTS-5-mediated aggrecan cleavage products in a dose-dependent fashion as compared to that of a nonselective hydroxamic acid inhibitor **14**[22] in our rat MIA model (Figure 5). Both modestly selective hydantoin **10** and highly selective hydantoin **13** had an ED_{50} of 30 mpk in this assay. Compound **11** had a slightly less robust performance, producing an ED_{50} at 75 mg/kg.

On the basis of the positive pharmacodynamic activity observed with compounds **10** and **13**, we next wanted to explore whether these aggrecanase inhibitors could also show efficacy in a surgical OA model. To that end, we studied compounds **10** and **13** in a rat meniscal tear model.[23] This model has been previously described and is a well-established acute model used to approximate human OA. Unlike our pharmacodynamic assay, the key readouts from the surgical model are histological assessments based on the comparison of knee joints with a surgically transected meniscus. Assessment of the joint structure then is expressed as a total joint score.[24] The dose−response data from the meniscal tear models is shown in Figures 6 and 7. To understand the predictive potential of the MIA model as a surrogate for the more resource-intensive meniscal tear model, we selected doses of our compounds that bracketed their MIA ED_{50}. Chronic BID dosing of both compounds **10** and **13** in the rat surgical model produced dose-dependent and statistically significant effects in overall total joint score. It is notable that enhanced metalloprotease selectivity in compound **13** did not result in any diminished ability to produce efficacy. We believe that the higher doses of compound **13** required to reach comparable activity to that of hydroxamate **14** have more to do with the significant difference in rat phamacokinetics between hydantoins **10** and **13** than to inherent protease selectivity (Table 2). Furthermore, in support of the hypothesis that the MIA model is a good surrogate to predict outcomes in the meniscal tear model, both compounds **10** and **13** produced statistically significant joint score effects similar in magnitude to that of nonselective hydroxamate **14** at doses equal to their MIA ED_{50}.

CONCLUSIONS

We were able to identify a series of hydantoins that inhibit both ADAMTS-4 and ADAMTS-5. We were able to optimize this

dx.doi.org/10.1021/jm501522n | J. Med. Chem. XXXX, XXX, XXX−XXX

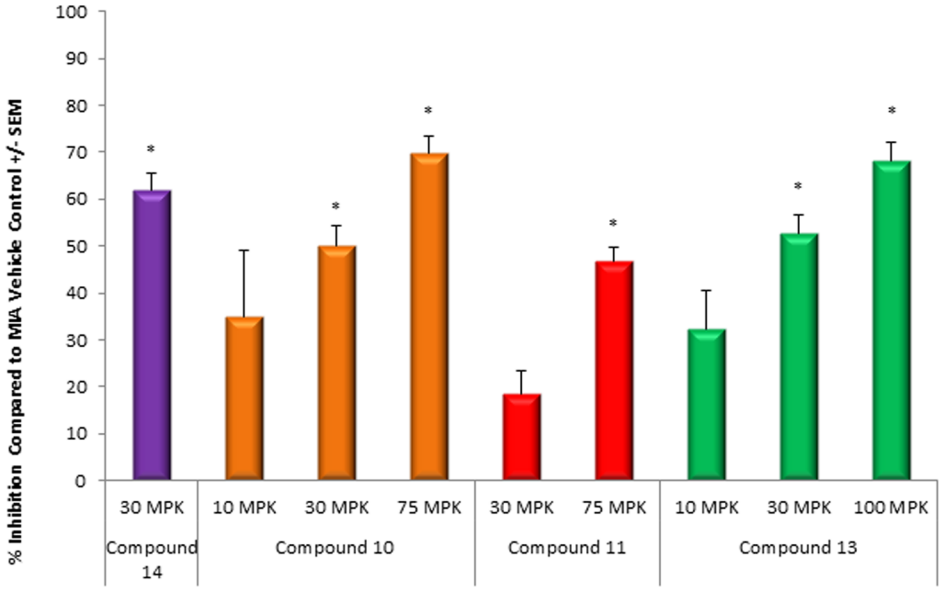

Figure 5. Percent inhibition of aggrecan cleavage in synovial fluid with hydantoins **10**, **11**, and **13** compared to that with hydroxamic acid **14** in the rat MIA model. Percent inhibition was determined by comparing amount of neoepitope in synovial fluid for compound-treated animals versus vehicle control. All compounds were dosed BID for 5 days prior to animal sacrifice and synovial fluid lavage. * indicates $p < 0.05$.

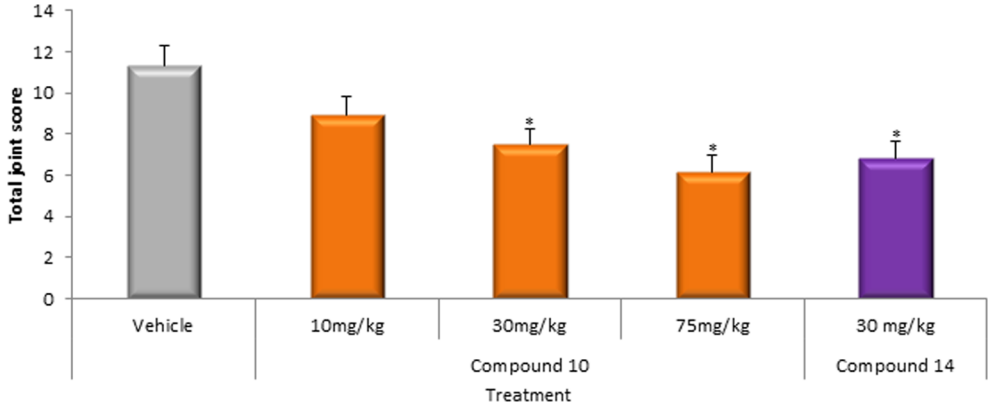

Figure 6. Effects in total joint score in the rat mensical tear model produced by treatment with hydantoin **10**. * indicates $p < 0.05$.

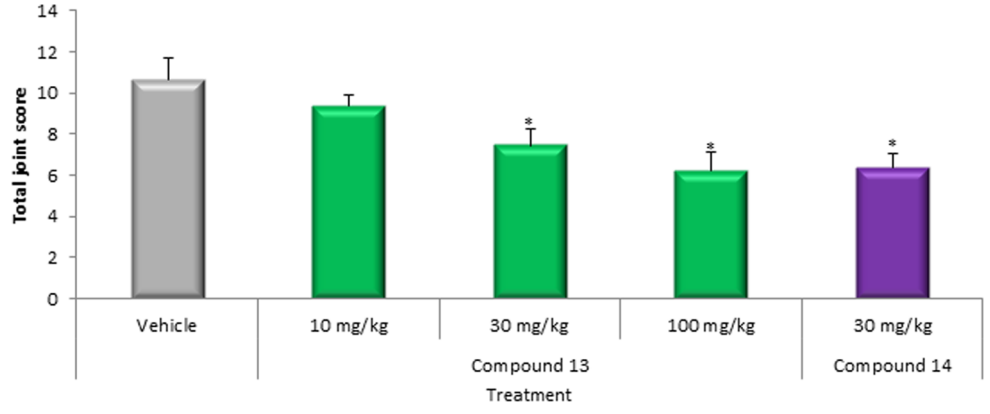

Figure 7. Effects in total joint score in the rat mensical tear model produced by treatment with hydantoin **13**. * indicates $p < 0.05$.

series using structure-based drug design to improve potency against ADAMTS-4 and ADAMTS-5 while at the same time improving the intrinsic selectivity versus a number of other zinc metalloproteases. Ultimately, compound **13** delivered the necessary levels of selectivity coupled with pharmacokinetic and pharmacodynamic performances to enable a proof-of-concept experiment in a rat meniscal tear model of OA. In this model, compound **13** showed altered progression of joint damage. These results are consistent with the work reported with ADAMTS-$5^{-/-}$ mice and the genetically modified mice producing aggrecan resistant to ADAMTS-5 cleavage. Our data further supports the hypothesis that selective ADAMTS-4/

dx.doi.org/10.1021/jm501522n | J. Med. Chem. XXXX, XXX, XXX−XXX

ADAMTS-5 inhibitors are valid targets for human DMOAD development. In addition, the data set described here supports the concept that the rat MIA model can be used to effectively predict compound success in the rat meniscal tear model, allowing quicker and more efficient compound in vivo assessments to be made.

EXPERIMENTAL SECTION

ADAMTS-4/ADAMTS-5 Biochemical Assay. Typically, 3 or 4 nM ADAMTS-4 or 2.1 nM ADAMTS-5 is incubated with 80 nM 43-mer peptide substrate (VQTVTWPDMELPLPRNITEGEARGSV-ILTVKPIFEVSPSPLKG) ± inhibitors (1% final DMSO concentration) for 3 h at room temperature in a white nonbinding surface 96-well plate (Corning 3990). Inhibitors are serially diluted 3-fold and tested at final starting concentrations of up to approximately 100 pM. The assay is then quenched with a cocktail containing EDTA (62.5 mM), 50 mM Tris(hydroxymethyl) aminomethane (Tris) (pH 7.5), 10 mM calcium chloride, 100 mM sodium chloride, 0.2 lo Brij (main component of polyoxyethylene(23) lauryl ether), 0.1% bovine serum albumin (BSA), BC3 monoclonal antibody hybridoma supernatant (1:2000 final dilution), streptavidin-conjugated donor beads, and anti-mouse IgG-conjugated acceptor beads (15 pg/mL final concentration for both beads). The plate is covered with aluminum foil tape, and the binding is allowed to incubate overnight. The plate is then read on an AlphaScreen Fusion Alpha reader from PerkinElmer. Data is analyzed using ActivityBase software (IDBS, Alameda, CA).

ADAMTS-5 Plasma Shift Assay. The assay is completed similar to the biochemical assay using 10 nM ADAMTS-5 and 50% Lewis rat plasma.

MMP and TACE Biochemical Assays. A continuous assay is used in which the substrate is the peptide Mca-PQGL-(3-[2,4-dinitrophenyl]-L-2,3-diaminopropionyl)-AR-OH. The assay buffer consists of 100 mM Tris-HC1 (pH 7.5), 100 mM NaC1, 10 mM $CaCl_2$, and 10 μM human serum albumin. Each well of the 96-well plate consists of a 100 μL reaction mixture consisting of assay buffer, MMP or TACE enzyme, and varied concentrations of inhibitor (prepared by serially diluting a given inhibitor in DMSO in a 96-well polypropylene plate using a 10 or 11 point dilution scheme). The enzymatic reactions are initiated by adding the substrate to a final concentration of 20 μM. The final DMSO concentration in the assay is 1.0%. The plate is incubated for 2−4 h at room temperature, and substrate cleavage is determined at room temperature with a fluorescence plate reader (excitation filter, 320 nm; emission filter, 436 nm) on a LJL Analyst or a Wallac Envision. The data is analyzed by using ActivityBase software (IDBS, Alameda, CA) ver. 5.3 using a 4 parameter fit model equation 205, from which relative IC_{50}'s are generated. Maximum signal is calculated from wells untreated by inhibitor but having enzyme, substrate, and 1.0% DMSO. Minimum signal is calculated from wells having buffer only (no enzyme), substrate, and 1.0% DMSO.

MIA Assay. This assay has been described in detail in the literature.[20] Briefly, MIA (sodium salt) is prepared fresh on the day of use at 3 mg in 50 μL of sterile 0.9% saline. 7 to 8 week-old male Lewis rats are anesthetized and injected intra-articularly with MIA into the right knee (to induce endogenous aggrecanase activity and the release of aggrecan fragments into the synovial fluid) and saline in the left (contralateral) knee on day 0. Aggrecanase inhibitor or vehicle [1% hydroxyethyl cellulose (HEC), 0.25% Tween 80, 0.05% antifoam] are dosed orally, twice a day, starting from day 3. A single dose of compound is given on day 7, the animals are sacrificed 4 h later, and the knee joints are lavaged with 200 μL of saline. The synovial lavage is assayed for aggrecanase-cleaved fragments of aggrecan using the NITEGE sandwich ELISA. The amount of aggrecan fragments present in the synovial lavage is determined on the basis of a standard curve generated with aggrecanase-digested rat aggrecan. Statistical analysis is performed using Dunnett's test.

Sandwich ELISA Assay. For the NITEGE ELISA, the a-NITEGE monoclonal antibody is immobilized on white high-binding ELISA plates (Nunc) overnight at 4 °C. Following blocking, rat synovial fluid lavage samples are added to the plate, and fragments with a C-terminal NITEGE sequence are captured. The captured fragments are detected using the HRP-conjugated a-HABR monoclonal antibody. The ELISA signal is measured using the Supersignal ELISA femto maximum sensitivity substrate (Pierce) and read on a Victor luminometer. The amount of aggrecan fragments present in the sample is determined on the basis of a standard curve generated with aggrecanase-digested rat chondrosarcoma aggrecan (850 mg/mL stock diluted in antibody dilution buffer).

Meniscal Tear (MT) Model. Two studies were run using male Lewis rats from Harlan, Indianapolis, aged between 17 and 20 weeks, with dosing beginning on day 0 and being twice daily at 5 mL/kg. In study one, male rats were dosed with compound **10** at 10, 30, and 75 mg/kg, compound **14** at 30 mg/kg, or vehicle (1% CMC in water, 0.25% Tween 80). In study two, rats were dosed with compound **13** at 10, 30, and 100 mg/kg, compound **14** at 30 mg/kg, or vehicle (1% HEC cellulose in water, 0.25% Tween-80, 0.05% antifoam). On day 1, after the morning dose, rats were anesthetized, and meniscal tear surgery was performed on the right knee, with the left knee left unoperated. Three weeks postsurgery, rats were euthanized, and the right knees were dissected out, decalcified, sectioned, and stained with toluidine blue. Stained sections were then scored for pathology, and a total joint score was reported. Surgery, staining, and scoring were performed as described in the literature.[24]

Microsomal Stability and Inhibition. Stability and inhibition were measured at 37 °C in a microsomal preparation using a Applied Biosystems Single Quad LC-MS. Microsomal concentrations for inhibition assays were 0.6 mg/mL for Cyp2D6, 0.13 mg/mL for Cyp3A4, and 0.3 mg/mL for Cyp2C9. Concentrations of microsomes was 1.11 mg/mL for both human and rat stability assays. Incubation times for inhibition assays were 3 min for Cyp3A4 and Cyp2D6 and 10 min for Cyp2C9. Incubation time for stability assays was 30 min, and compound concentrations were 4 μM.

Chemistry General methods. ^{1}H and ^{13}C NMR spectra were measured at 400 MHz on a Varian spectrometer unless indicated otherwise. All solvents were dry and obtained as such from commercial sources. Reagents were obtained from commercial sources and used as received. Purity of final compounds used in biological assays was determined by electrospray LCMS to be ≥95% for compounds studied in biological assays. Compounds were dissolved in DMSO, water, or methanol and injected (1 μL) into an Agilent Infinity HPLC (3 μm 50 × 2 mm C18 column, 1.2 mL/min, gradient 5 to 95% acetonitrile/0.1% formic acid over 8 min) coupled to an Agilent 6150 quadropole MS. Percent purity was determined for the peak corresponding to the molecular ion at 214 and 300 nM.

DANGER: *Potassium cyanide and hydrogen cyanide gas are highly toxic*! Ensure that all acidic reagents have been removed from the reaction vicinity in case of accidental release of cyanide. Perform reactions only in well-ventilated fume hoods. Under heating, these hydantoin forming reactions generate substantial pressure! Use blast shields and other appropriate safety precautions when handling. During the reaction, the ammonium salts can sublime and collect above the solvent, which may prevent adequate venting of the reactions depending on the vessel shape/size and venting mechanisms: *use extreme caution when handling vessels that have been heated, and vent away from people*. Ideally, a reaction vessel will have an internal pressure sensor to ensure venting has occurred prior to handling. On the basis of our experience, glass vessels such as Parr bottles may be unable to contain the pressure of the reactions depending on the scale, age of the vessel, and other factors. Use of nonglass vessels rated for HIGH pressure is preferred.

General Procedure for Preparation of Ketones (3a−e). Dissolve [(methoxy-methyl-carbamoyl)-methyl]-carbamic acid *tert*-butyl ester **2** (5.0 g, 22.91 mmol) in THF (48 mL) and cool to −25 °C for Grignard additions and −78 °C for addition of lithiates. Add slowly, via syringe, the corresponding Grignard or lithium reagent (2 equiv in THF) and stir 1 h. Warm to ambient temperature and stir overnight. Quench with 1.0 N hydrochloric acid, extract with diethyl ether (3×), dry over solid sodium sulfate, and concentrate under reduced pressure to give the crude product. Purify with flash column chromatography, eluting with an EtOAc in hexanes gradient.

dx.doi.org/10.1021/jm501522n | J. Med. Chem. XXXX, XXX, XXX−XXX

(2-Oxo-2-phenyl-ethyl)-carbamic Acid *tert*-Butyl Ester (3a). Prepared from PhMgBr (5.15 g, 96%) as a clear colorless oil using the general procedure. Analytical data were consistent with previously published data.[25]

***tert*-Butyl *N*-[2-(3-Methyl-2-pyridyl)-2-oxo-ethyl]carbamate (3b).** 2-Bromo-3-methylpyridine (10 mL, 89.64 mmol) was dissolved in dry tetrahydrofuran (50 mL) and cooled to −10 °C under nitrogen. Isopropylmagnesium chloride solution (1 equiv, 44.82 mL, 2 M in THF) was added. The reaction was stirred at −10 °C for 1 h and then warmed to ambient temperature and stirred for an additional 2 h. The reaction was warmed to 45 °C and stirred overnight. The resulting aryl magnesium reagent solution was cooled to ambient temperature.

In a separate flask, Weinreb amide 2 (89.64 mmol, 19.56 g) was suspended in dry tetrahydrofuran (50 mL) under nitrogen and cooled to −70 °C. Isopropylmagnesium chloride solution (1 equiv, 44.82 mL, 2 M in THF) was added slowly. After the mixture became homogeneous, it was warmed to ambient temperature, and the pyridine Grignard reagent was added via cannula. Mixture was stirred overnight. Reaction was poured into EtOAc and washed with saturated NH_4Cl solution (×2) and brine, dried over Na_2SO_4, filtered, and concentrated. Residue was purfied by flash chromatography (0 to 100% EtOAc/hexanes) to give the title compound (4.49 g; 20.01% yield) as a yellow solid. MS: ES(+) = 251.3 *m*/*z* (M + H); ^{1}H NMR ($CDCl_3$, 400 MHz) 8.48 (d, *J* = 3.6 Hz, 1H), 7.58 (d, *J* = 8.0 Hz, 1H), 7.35 (dd, *J* = 8.0, 4.8 Hz, 1H), 5.34 (bs, 1H), 4.81 (d, *J* = 4.8 Hz, 2H), 2.59 (s, 3H), 1.45 (s, 9H).

(2-Oxo-2-thiazol-2-yl-ethyl)-carbamic Acid *tert*-Butyl Ester (3c). Thiazole (17.8 mL, 252 mmol) was dissolved in dry THF (50 mL) and cooled in an acetonitrile/dry ice bath to −35 to −45 °C. The solution was treated dropwise with *n*-BuLi in hexane (2.5 M, 100 mL, 252 mmol). After 45 min at −30 to −45 °C, a solution of *tert*-butyl 2-(methoxy(methyl)amino)-2-oxoethylcarbamate (25 g, 114.5 mmol) in 200 mL of THF was added dropwise, via cannula, while keeping the temperature below −30 °C. After 1.5 h at −30 to −40 °C, the reaction was quenched with 1 N citric acid (120 mL) and diluted with EtOAc. The layers were separated. The aqueous layer was extracted once more, and the organic extracts were combined, washed with brine, dried over $MgSO_4$, filtered, and concentrated. The crude in was dissolved dichloromethane with a small amount of EtOAc and purified by silica gel chromatography, eluting with an isocratic system of 25% EtOAc/hexane for 30 min and 25−60% EtOAc/hexane over 30 min to give the title compound (19.3 g, 71%). ES/MS (*m*/*z*): 187 (M − *t*-butyl + 1). ^{1}H NMR ($CDCl_3$, 400 MHz) 8.0 (d, *J* = 2.8 Hz, 1H), 7.70 (d, *J* = 3.2 Hz, 1H), 5.26 (bs, 1H), 4.79 (d, *J* = 5.2 Hz, 2H), 1.45 (s, 9H).

***tert*-Butyl *N*-[2-(1-Methylimidazol-2-yl)-2-oxo-ethyl]-carbamate (3d).** To a 5 L flask under a nitrogen atmosphere was added 1-methylimidazole (0.71 kg; 8.7 mol) and tetrahydrofuran (6.5 L). The mixture was chilled to −68 °C and a butyl lithium solution (3.5 L, 8.8 mol) was added slowly over a period of 3 h via addition funnel. After addition, the mixture was stirred cold for 20 min. Amide **2** (0.85 kg; 3.9 mol) was added in portions such that the internal temperature did not rise above −55 °C. The mixture was then slowly warmed to −14 °C. Saturated ammonium chloride solution (3.0 L) was added, and the mixture was cannulated to a 22 L separatory funnel filled with 8 L of water. The cloudy turbid mixture was diluted with dichloromethane (7 L). The organic layer was separated and concentrated to a white solid. The solid was slurred in 4.0 L of 20% ethyl acetate/heptane. The suspension was filtered to give the title compound as a white solid (801 g, 87%). ^{1}H NMR (DMSO-d_6, 400 MHz) 7.51 (s, 1H), 7.10 (s, 1H), 6.97 (t, *J* = 6.2 Hz, 1H), 4.39 (d, *J* = 6.2 Hz, 2H), 3.90 (s, 3H), 1.38 (s, 9H).

***tert*-Butyl *N*-[2-(2-Methylpyrazol-3-yl)-2-oxo-ethyl]-carbamate (3e).** The lithiated pyrrazole was prepared as described previously.[26] Coupling to the Weinreb amide was conducted using the general procedure. Clear oil (750 mg, 36%). ^{1}H NMR ($CDCl_3$, 400 MHz) 7.46 (d, *J* = 2.2 Hz, 1H), 6.85 (d, *J* = 2.2 Hz, 1H), 5.28 (d, *J* = 14.1 Hz, 1H), 4.45 (d, *J* = 4.8 Hz, 2H), 4.15 (s, 3H), 1.44 (s, 9H).

General Procedure for the Synthesis of *N*-Boc-Hydantoins (4a−e). Dissolve ketone (3) in ethanol (7 mL/mmol ketone) in a pressure vessel. Add water (2 mL/mmol of ketone), KCN (2 equiv), and ammonium carbonate (2 equiv), seal, and heat at 80 °C until the reaction is complete (typically overnight to 1−2 days). [**Caution − High pressure will be generated.**] Cool reaction, add an equal volume of water, and concentrate under reduced pressure to remove ethanol. Filter the aqueous mixture, rinse with water (5×), and air-dry to give hydantoin compound **4**.

***tert*-Butyl *N*-[(2,5-Dioxo-4-phenyl-imidazolidin-4-yl)methyl]-carbamate (4a).** White solid (190g, 85%). ^{1}H NMR (400 MHz, DMSO-d_6) 10.74−10.67 (m, 1H), 8.25 (s, 1H), 7.50−7.48 (m, 2H), 7.36−7.27 (m, 3H), 6.88 (m, 1H), 3.58−3.53 (m, 2H), 1.29 (s, 9H).

***tert*-Butyl *N*-[[4-(3-Methyl-2-pyridyl)-2,5-dioxo-imidazolidin-4-yl]methyl]carbamate (4b).** White solid (4.3 g, 73%). ^{1}H NMR (400 MHz, DMSO-d_6) 10.94 (s, 1H), 8.38 (dd, *J* = 1.3, 4.8 Hz, 1H), 8.02 (s, 1H), 7.60 (d, *J* = 7.0 Hz, 1H), 7.29 (dd, *J* = 4.8, 7.5 Hz, 1H), 6.59−6.55 (m, 1H), 3.92−3.79 (m, 2H), 2.17 (s, 3H), 1.34 (s, 9H).

***tert*-Butyl *N*-[(2,5-Dioxo-4-thiazol-2-yl-imidazolidin-4-yl)-methyl]carbamate (4c).** Prepared according to the general procedure but using MeOH rather than the EtOH/water mixture and heating at 35 °C. White solid (230 g, 85%). ^{1}H NMR (400 MHz, DMSO-d_6) 11.10 (bs, 1H), 8.50 (bs, 1H), 7.81 (s, 1H), 7.80 (s, 1H), 7.05 (bs, 1H), 3.94−3.91 (m, 2H), 1.32 (s, 9H).

***tert*-Butyl *N*-[[4-(1-Methylimidazol-2-yl)-2,5-dioxo-imidazolidin-4-yl]methyl]carbamate (4d).** White solid (14g, 51%). ^{1}H NMR (400 MHz, DMSO-d_6) 11.06 (s, 1H), 8.13 (s, 1H), 7.16 (s, 1H), 6.82−6.76 (m, 2H), 3.79 (d, *J* = 5.7 Hz, 2H), 3.45 (s, 3H), 1.34 (s, 9H).

***tert*-Butyl *N*-[[4-(2-Methylpyrazol-3-yl)-2,5-dioxo-imidazolidin-4-yl]methyl]carbamate (4e).** White solid (180 mg, 23%). ^{1}H NMR (400 MHz, DMSO-d_6) 11.05 (s, 1H), 8.13 (s, 1H), 7.32 (d, *J* = 2.2 Hz, 1H), 7.16−7.00 (m, 1H), 6.39 (d, *J* = 2.2 Hz, 1H), 3.72 (s, 3H), 3.62 (d, *J* = 6.6 Hz, 2H), 1.32 (s, 11H).

Chiral Separation of Hydantoins 4a−e. The enantiomers of racemic hydantoins **4a−e** can be separated using chiral chromatography: column, 8 × 36 cm Chiralpak AD, 20 μm; flow rate, 400 mL/min; detection, 250 nm; mobile phase, methanol or 3A ethanol. (The addition of acetonitrile (5−40%) was required in some instances.)

General Procedure for Synthesis of Hydantoins (7−13). The protected hydantoins (**5a−e**) were dissolved in MeOH and treated with excess 4 M HCl·dioxane at 0 °C. Upon consumption of the starting material, the reaction was concentrated to give the HCl salt (**6a−e**), which was used directly in the next reaction.

The hydantoin HCl salt (**6a−e**) was combined in dry DMF with PyBroP (1.3 equiv), the benzofuran carboxylic acid (1.5 equiv), and diisopropylethylamine (3 equiv) in a flask and heated at 80 °C for 1 h. The reaction was cooled to ambient temperature and concentrated onto silica. Flash chromatography (gradient 0−100% EtOAc/hexane) gave the title compounds (**7−13**).

5-Chloro-*N*-[[4-methyl-2,5-dioxo-imidazolidin-4-yl]methyl]-benzofuran-2-carboxamide (7). White solid (86 mg, 25%). ^{1}H NMR (400 MHz, DMSO-d_6) 10.62 (s, 1H), 8.68 (t, *J* = 6.4 Hz, 1H), 7.86−7.81 (m, 2H), 7.69−7.64 (m, 1H), 7.55−7.53 (m, 1H), 7.49−7.44 (m, 1H), 3.53−3.41 (m, 2H), 1.24 (s, 3H).

5-Chloro-*N*-[[(4R)-2,5-dioxo-4-phenyl-imidazolidin-4-yl]-methyl]benzofuran-2-carboxamide (8). $[\alpha]_D^{20}$ = +70° (*c* 1.0, MeOH). White solid (280 mg, 60%). ^{1}H NMR (400 MHz, DMSO-d_6) 10.81 (s, 1H), 8.70 (t, *J* = 6.2 Hz, 1H), 8.49 (s, 1H), 7.84 (d, *J* = 2.2 Hz, 1H), 7.65 (d, *J* = 9.0 Hz, 1H), 7.56−7.54 (m, 2H), 7.51 (d, *J* = 0.9 Hz, 1H), 7.44 (dd, *J* = 2.2, 8.8 Hz, 1H), 7.39−7.35 (m, 2H), 7.32−7.28 (m, 1H), 3.90 (dd, *J* = 2.3, 6.3 Hz, 2H).

5-Chloro-*N*-[[4-(3-methyl-2-pyridyl)-2,5-dioxo-imidazolidin-4-yl]methyl]benzofuran-2-carboxamide (9). White solid (170 mg, 50%). ^{1}H NMR (399.81 MHz, DMSO-d_6) 11.11−11.01 (m, 1H), 8.51−8.46 (m, 3H), 8.26 (s, 1H), 7.85 (d, *J* = 2.2 Hz, 1H), 7.69−7.65 (m, 3H), 7.53 (s, 1H), 7.46 (dd, *J* = 2.4, 9.0 Hz, 1H), 7.36 (dd, *J* = 4.6, 7.7 Hz, 1H), 4.28 (dd, *J* = 6.2, 13.6 Hz, 1H), 4.20−4.16 (m, 1H), 2.19 (s, 3H).

5-Chloro-*N*-[[(4R)-2,5-dioxo-4-thiazol-2-yl-imidazolidin-4-yl]methyl]benzofuran-2-carboxamide (10). White solid (4.7 g, 77%). $[\alpha]^{20}_D$ = +76° (c 1.0, MeOH). ^{1}H NMR (400 MHz, DMSO-d_6) 11.07 (s, 1H), 8.82 (t, *J* = 6.2 Hz, 1H), 8.79 (d, *J* = 1.3 Hz, 1H), 7.87

dx.doi.org/10.1021/jm501522n | J. Med. Chem. XXXX, XXX, XXX−XXX

(d, J = 3.1 Hz, 2H), 7.80 (d, J = 3.1 Hz, 1H), 7.69 (d, J = 9.2 Hz, 1H), 7.57 (s, 1H), 7.48 (dd, J = 2.4, 9.0 Hz, 1H), 7.25−7.11 (m, 2H), 4.25−4.02 (m, 2H). ^{13}C NMR (100 MHz, DMSO-d_6): 172.32, 166.53, 158.85, 156.85, 153.15, 150.20, 143.82, 129.03, 128.53, 127.42, 122.69, 122.29, 113.97, 110.08, 68.76.

5-Chloro-*N*-[[(4S)-4-(1-methylimidazol-2-yl)-2,5-dioxo-imidazolidin-4-yl]methyl]benzofuran-2-carboxamide (11). White solid (2.7 g, 66%). $[\alpha]_D^{20}$ = +44° (c 1.0, MeOH). ^{1}H NMR (399.81 MHz, DMSO-d_6) 11.19 (s, 1H), 8.65 (t, J = 6.4 Hz, 1H), 8.39 (s, 1H), 7.85 (d, J = 1.8 Hz, 1H), 7.68 (d, J = 8.8 Hz, 1H), 7.53 (s, 1H), 7.46 (dd, J = 2.0, 9.0 Hz, 1H), 7.22 (s, 1H), 6.90 (s, 1H), 4.21−4.11 (m, 2H), 3.47 (s, 3H). ^{13}C NMR (100 MHz, DMSO-d_6) 173.16, 158.69, 156.76, 153.11, 150.38, 141.45, 129.09, 128.54, 127.41, 126.70, 125.02, 122.66, 113.97, 109.95, 64.64, 33.08.

5-Chloro-*N*-[[4-(2-methylpyrazol-3-yl)-2,5-dioxo-imidazolidin-4-yl]methyl]benzofuran-2-carboxamide (12). White solid (75 mg, 31%). ^{1}H NMR (400 MHz, DMSO-d_6) 11.25 (s, 1H), 8.85−8.82 (m, 2H), 8.35 (s, 1H), 7.86 (d, J = 2.2 Hz, 1H), 7.67 (d, J = 8.8 Hz, 1H), 7.55 (s, 1H), 7.46 (dd, J = 2.2, 8.8 Hz, 1H), 7.35 (d, J = 1.8 Hz, 1H), 6.50 (d, J = 1.8 Hz, 1H), 4.07−3.95 (m, 2H), 3.76 (s, 3H).

***N*-[[(4S)-4-(1-methylimidazol-2-yl)-2,5-dioxo-imidazolidin-4-yl]methyl]-5-(trifluoromethyl)benzofuran-2-carboxamide (13).** White solid (6.1 g, 28%). $[\alpha]_D^{20}$ = +44° (c 1.0, MeOH). ^{1}H NMR (400 MHz, DMSO-d_6) 11.23 (s, 1H), 8.76 (t, J = 6.4 Hz, 1H), 8.44 (s, 1H), 8.24 (s, 1H), 7.88 (d, J = 8.8 Hz, 1H), 7.78 (dd, J = 2.0, 9.0 Hz, 1H), 7.71 (s, 1H), 7.24 (s, 1H), 6.93 (s, 1H), 4.26−4.15 (m, 2H), 3.50 (s, 3H). ^{13}C NMR (100 MHz, DMSO-d_6) 173.18, 158.60, 156.76, 156.04 (m), 150.78, 141.45, 127.85, 126.75, 126.24, 125.36, 125.01 (m), 123.53, 113.47, 110.55, 64.64, 33.05.

■ ASSOCIATED CONTENT

Ⓢ Supporting Information

Experimental details for X-ray co-crystallization and computational studies. This material is available free of charge via the Internet at http://pubs.acs.org.

Accession Codes

X-ray data is available through the PDB database (www.pdb.org) under accession codes 4KW7, 4KWE, and 4KWI.

■ AUTHOR INFORMATION

Corresponding Author

*E-mail: durhamti@lilly.com; Phone: 317-433-8447; Fax: 317-433-0552.

Author Contributions

Design of inhibitors: T.B.D, V.J.K, J.M., C.J.R., J.L.T., and M.R.W. Synthesis of inhibitors: T.B.D, J.M., C.J.R., J.L.T., and C.L. Design of in vivo biological experiments: T.B.D., L.A., K.T., M.G.C, and M.R.W. Development of biochemical and biomarker assays: C.S. and K.T. Conducting the MIA and meniscal tear experiments: C.L. Computational analysis: V.J.K. X-ray crystallography: J.D.D. and S.L.S.

Notes

The authors declare the following competing financial interest(s): All of the authors are employees and shareholders of Eli Lilly and Company.

■ ACKNOWLEDGMENTS

Use of the Advanced Photon Source, an Office of Science User Facility operated for the U.S. Department of Energy (DOE) Office of Science by Argonne National Laboratory, was supported by the U.S. DOE under contract no. DE-AC02-06CH11357. Use of the Lilly Research Laboratories Collaborative Access Team (LRL-CAT) beamline at Sector 31 of the Advanced Photon Source was provided by Eli Lilly Company, which operates the facility.

■ ABBREVIATIONS USED

OA, osteoarthritis; ECM, extracellular matrix; MIA, monoiodoacetate; ADAMTS, a disintegrin and metalloproteinase with thrombospondin motifs; DMOAD, a disease-modifying OA drug

■ REFERENCES

(1) Lawrence, R. C.; Felson, D. T.; Helmick, C. G.; Arnold, L. M.; Choi, H.; Deyo, R. A.; Gabriel, S.; Hirsch, R.; Hochberg, M. C.; Hunder, G. G.; Jordan, J. M.; Katz, J. N.; Kremers, H. M.; Wolfe, F. Estimates of the prevalence of arthritis and other rheumatic conditions in the United States. Part II. *Arthritis Rheum.* **2008**, *58*, 26−35.

(2) Lopez, A. D.; Mathers C. D.; Ezzati M.; Jamison D. T.; Murray C. J. L. Global and regional burden of disease and risk factors, 2001: systematic analysis of population health data. *Lancet 367*, 1747−1757.

(3) Woolf, A. D.; Pfleger, B. Burden of major musculoskeletal conditions. *Bull. WHO* **2003**, *81*, 646−56.

(4) Chen, A.; Gupte, C.; Akhtar, K.; Smith, P.; Cobb, J. The global economic cost of osteoarthritis: how the UK compares. *Arthritis* **2012**, *2012*, 698−709.

(5) Simkin, P. A.; Pizzorno, J. E. Transynovial exchange of small molecules in normal human subjects. *J. Appl. Physiol.* **1974**, *36*, 581−587.

(6) (a) Horkay, F.; Basser, P. J. Cartilage proteoglycans: structure, assembly and organization. *PMSE Prepr.* **2011**, *104*, 286−287. (b) Hardingham, T. E.; Fosang, A. J. The structure of aggrecan and its turnover in cartilage. *J. Rheumatol., Suppl.* **1995**, *43*, 86−90.

(7) Settle, S.; Vickery, L.; Nemirovskiy, O.; Vidmar, T.; Bendele, A.; Messing, D.; Ruminski, P.; Schnute, M.; Sunyer, T. Cartilage degradation biomarkers predict efficacy of a novel, highly selective matrix metalloproteinase 13 inhibitor in a dog model of osteoarthritis. *Arthritis Rheum.* **2010**, *62*, 3006−3015.

(8) Sumer, E. U.; Qvist, P.; Tanko, L. B. Matrix metalloproteinase and aggrecanase generated aggrecan fragments: implications for the diagnostics and therapeutics of destructive joint diseases. *Drug Dev. Res.* **2007**, *68*, 1−13.

(9) Malemud, C. J. Matrix metalloproteinases (MMPs) in health and disease: an overview. *Front. Biosci.* **2006**, *11*, 1696−1701.

(10) Peterson, J. T. The importance of estimating the therapeutic index in the development of matrix metalloproteinase inhibitors. *Cardiovasc. Res.* **2006**, *69*, 677−687.

(11) (a) Lohmander, L. S.; Neame, P. J.; Sandy, J. D. The structure of aggrecan fragments in human synovial fluid. Evidence that aggrecanase mediates cartilage degradation in inflammatory joint disease, joint injury, and osteoarthritis. *Arthritis Rheum.* **1993**, *36*, 1214−22. (b) Sandy, J. D.; Flannery, C. R.; Neame, P. J.; Lohmander, L. S. The structure of aggrecan fragments in human synovial fluid. Evidence for the involvement in osteoarthritis of a novel proteinase which cleaves the Glu 373−Ala 374 bond of the interglobular domain. *J. Clin. Invest.* **1992**, *89*, 1512−16.

(12) (a) Glasson, S. S.; Askew, R.; Sheppard, B.; Carito, B.; Blanchet, T.; Ma, H.-L.; Flannery, C. R.; Peluso, D.; Kanki, K.; Yang, Z.; Majumdar, M. K.; Morris, E. A. Deletion of active ADAMTS5 prevents cartilage degradation in a murine model of osteoarthritis. *Nature* **2005**, *434*, 644−648. (b) Li, J.; Anemaet, W.; Diaz, M. A.; Buchanan, S.; Tortorella, M.; Malfait, A. M.; Mikecz, K.; Sandy, I. D.; Plaas, A. Knockout of ADAMTS5 does not eliminate cartilage aggrecanase activity but abrogates joint fibrosis and promotes cartilage aggrecan deposition in murine osteoarthritis models. *J. Orthop. Res.* **2011**, *29*, 516−522.

(13) Little, C. B.; Meeker, C. T.; Golub, S. B.; Lawlor, K. E.; Farmer, P. J.; Smith, S. M.; Fosang, A. J. Blocking aggrecanase cleavage in the aggrecan interglobular domain abrogates cartilage erosion and promotes cartilage repair. *J. Clin. Invest.* **2007**, *117*, 1627−1636.

(14) (a) Glasson, S. S.; Askew, R.; Sheppard, B.; Carito, B. A.; Blanchet, T.; Ma, H.-L.; Flannery, C. R.; Kanki, K.; Wang, E.; Peluso, D.; Yang, Z.; Majumdar, M. K.; Morris, E. A. Characterization of and osteoarthritis susceptibility in ADAMTS-4-knockout mice. *Arthritis Rheum.* **2004**, *50*, 2547−2558. (b) Stanton, H.; Rogerson, F. M.; East, C. J.; Golub, S. B.; Lawlor, K. E.; Meeker, C. T.; Little, C. B.; Last, K.; Farmer, P. J.; Campbell, I. K.; Fourie, A. M.; Fosang, A. J. ADAMTS5 is the major aggrecanase in mouse cartilage in vivo and in vitro. *Nature* **2005**, *434*, 648−652.

(15) Song, R.-H.; Tortorella, M. D.; Malfait, A.-M.; Alston, J. T.; Yang, Z.; Arner, E. C.; Griggs, D. W. Aggrecan degradation in human articular cartilage explants is mediated by both ADAMTS-4 and ADAMTS-5. *Arthritis Rheum.* **2007**, *56*, 575−585.

(16) (a) Gilbert, A. M.; Bikker, J. A.; O'Neil, S. V. Advances in the development of novel aggrecanase inhibitors. *Expert Opin. Ther. Pat.* **2011**, *21*, 1−12. (b) De Rienzo, F.; Saxena, P.; Filomia, F.; Caselli, G.; Colace, F.; Stasi, L.; Giordani, A.; Menziani, M. C. Progress towards the identification of new aggrecanase inhibitors. *Curr. Med. Chem.* **2009**, *16*, 2395−2415.

(17) Meusel, M.; Guetschow, M. Recent developments in hydantoin chemistry. A review. *Org. Prep. Proced. Int.* **2004**, *36*, 391−443.

(18) Fernandez-Catalan, C.; Bode, W.; Huber, R.; Turk, D.; Calvete, J. J.; Lichte, A.; Tschesche, H.; Maskos, K. Crystal structure of the complex formed by the membrane type 1-matrix metalloproteinase with the tissue inhibitor of metalloproteinases-2, the soluble progelatinase A receptor. *EMBO J.* **1998**, *17*, 5238−5248.

(19) Dunten, P.; Kammlott, U.; Crowther, R.; Levin, W.; Foley, L. H.; Wang, P.; Palermo, R. X-ray structure of a novel matrix metalloproteinase inhibitor complexed to stromelysin. *Protein Sci.* **2001**, *10*, 923−926.

(20) Swearingen, C. A.; Chambers, M. G.; Lin, C.; Marimuthu, J.; Rito, C. J.; Carter, Q. L.; Dotzlaf, J.; Liu, C.; Chandrasekhar, S.; Duffin, K. L.; Mitchell, P. G.; Durham, T. B.; Wiley, M. R.; Thirunavukkarasu, K. A short-term pharmacodynamic model for monitoring aggrecanase activity: injection of monosodium iodoacetate (MIA) in rats and assessment of aggrecan neoepitope release in synovial fluid using novel ELISAs. *Osteoarthritis Cartilage* **2010**, *18*, 1159−1166.

(21) Swearingen, C. A.; Carpenter, J. W.; Siegel, R.; Brittain, I. J.; Dotzlaf, J.; Durham, T. B.; Toth, J. L.; Laska, D. A.; Marimuthu, J.; Liu, C.; Brown, D. P.; Carter, Q. L.; Wiley, M. R.; Duffin, K. L.; Mitchell, P. G.; Thirunavukkarasu, K. Development of a novel clinical biomarker assay to detect and quantify aggrecanase-generated aggrecan fragments in human synovial fluid, serum and urine. *Osteoarthritis Cartilage* **2010**, *18*, 1150−1158.

(22) (a) Noe, M. C.; Natarajan, V.; Snow, S. L.; Wolf-Gouveia, L. A.; Mitchell, P. G.; Lopresti-Morrow, L.; Reeves, L. M.; Yocum, S. A.; Otterness, I.; Bliven, M. A.; Carty, T. J.; Barberia, J. T.; Sweeney, F. J.; Liras, J. L.; Vaughn, M. Discovery of 3-OH-3-methylpipecolic hydroxamates: potent orally active inhibitors of aggrecanase and MMP-13. *Bioorg. Med. Chem. Lett.* **2005**, *15*, 3385−3388. (b) Noe, M. C.; Letavic M. A.; Hawkins J. M. Preparation of *N*-(*p*-benzyloxybenzenesulfonylamino)piperidine and -piperazine derivatives as selective inhibitors of aggrecanase in osteoarthritis treatment. EP1081137A1, 2001.

(23) Bendele, A. M. Animal models of rheumatoid arthritis. *J. Musculoskeletal Neuronal Interact.* **2001**, *1*, 377−385.

(24) Gerwin, N.; Bendele, A. M.; Glasson, S.; Carlson, C. S. The OARSI histopathology initiative—recommendations for histological assessments of osteoarthritis in the rat. *Osteoarthritis Cartilage* **2010**, *18*, S24−S34.

(25) Patonay, T.; Micskei, K.; Juhasz-Toth, E.; Fekete, S.; Pardi-Toth, V. C. α-Azido ketones, Part 6. Reduction of acyclic and cyclic α-azido ketones into α-amino ketones: old problems and new solutions. *ARKIVOC (Gainesville, FL, U.S.)* **2008**, 270−290.

(26) Balle, T.; Begtrup, M.; Jaroszewski, J. W.; Liljefors, T.; Norrby, P.-O. Regioselectivity in lithiation of 1-methylpyrazole: experimental, density functional theory and multinuclear NMR study. *Org. Biomol. Chem.* **2006**, *4*, 1261−1267.